Research Article

Abdul Habib, Salit Mohd Sapuan*, Edi Syams Zainudin, and Afdzaluddin Atiqah

Morphological, physical, thermal, and mechanical properties of carbon nanotubes reinforced arrowroot starch composites

https://doi.org/10.1515/ntrev-2025-0216
received October 25, 2024; accepted September 3, 2025

Abstract: It is necessary to uniformly disperse carbon-based nanoparticles within a biopolymer matrix. However, in most cases, carbon nanotubes (CNTs) tend to form agglomerates within the biopolymer matrix due to their hydrophobicity, lack of compatibility, and weak interfacial interaction with the matrix. This study involved the fabrication of nanocomposite films utilizing a simple solution casting approach. The films were made from plasticized starch derived from arrowroot starch (ARS) and multi-walled CNTs. Different amounts of CNTs (0–1 wt%) were used in the films. The CNTs were subjected to ultrasonic treatment to reach a uniform dispersion within the arrowroot starch. The ARS/CNTs nanocomposite films were characterized by physical properties, Fourier Transform Infrared Spectroscopy, X-ray diffraction, Thermogravimetric analysis, and mechanical properties. The presence of CNTs effectively restricts the paths available for water molecules, resulting in an enhanced water barrier. The tensile strength of 1% CNTs-reinforced film was 9.14 MPa (increased by 174%). This suggests improved dispersion of CNTs in the ARS matrix as a result of the establishment of strong hydrogen bonds with the ARS matrix. Furthermore, this also demonstrates the effectiveness of ARS as a biopolymer, since it has the ability to form strong bonds with the CNTs filler without causing agglomeration inside the matrix.

Keywords: dispersion, carbon nanotubes, arrowroot starch

*** Corresponding author: Salit Mohd Sapuan,** Advanced Engineering Materials and Composites Research Centre (AEMC), Department of Mechanical and Manufacturing Engineering, Universiti Putra Malaysia, UPM Serdang, Selangor, 43400, Malaysia, e-mail: sapuan@upm.edu.my
Abdul Habib: Advanced Engineering Materials and Composites Research Centre (AEMC), Department of Mechanical and Manufacturing Engineering, Universiti Putra Malaysia, UPM Serdang, Selangor, 43400, Malaysia
Edi Syams Zainudin: Advanced Engineering Materials and Composites Research Centre (AEMC), Department of Mechanical and Manufacturing Engineering, Universiti Putra Malaysia, UPM Serdang, Selangor, 43400, Malaysia; Laboratory of Biocomposite Technology, Institute of Tropical Forestry and Forest Products (INTROP), Universiti Putra Malaysia, UPM Serdang, Selangor, 43400, Malaysia
Afdzaluddin Atiqah: Institute of Microengineering and Nanoelectronics (IMEN), Universiti Kebangsaan Malaysia, UKM, Bangi, Selangor, Malaysia

1 Introduction

The advancement of sustainable materials generated from bio-sources has increased significantly in recent years due to the global environmental and resource issues caused by plastics originating from petroleum. Starch is a biopolymer extracted from a wide range of crops as promising materials for the production of biodegradable plastics [1]. Starch and other natural biopolymers are excellent replacements for packaging made of commercially available synthetic biopolymers. Starch may be used to create packaging materials, particularly films with their excellent transparency, limited moisture absorption, and appropriate strength [2,3].

Starch is a naturally occurring polymer with a large molecular weight and multiple hydroxyl groups, which form hydrogen bonds with neighboring molecules [4]. When compared to synthetic biodegradable polymers, natural biopolymers are much more advantageous since they are completely compostable without leaving any harmful residue and are readily accessible, renewable, and inexpensive. Thermoplastic materials made from starch are promising alternatives for creating bio-based materials because of their abundant supply and renewable nature [5]. Among various starches, arrowroot starch (ARS), locally produced in Indonesia and Malaysia, stands out for its unique digestibility, gel-forming ability, and high amylose content (40.86%), which plays a crucial role in developing stronger and stiffer films [6]. Studies have shown that the high amylose content of ARS, through hydrogen bonding between linear chains, results in stronger films compared to other starch sources, making it a valuable material for bio-based applications [7]. Nevertheless, the inferior mechanical qualities, barrier properties, and thermal stability have regrettably fallen short compared to traditional petroleum-based

plastics [8]. The development of nanotechnology also demonstrates that the reinforcement of nanofillers into the plasticizer starch has been proven to be effective to improve material properties and performance of biopolymers [9].

Carbon nanotubes (CNTs) have gained considerable focus among researchers in the field of nano-carbon-based composites. CNTs are regarded as exemplary materials owing to their extensive surface area, elevated aspect ratio, and remarkable material characteristics for the production of composite materials [10]. Even small amounts of CNTs have been proven to improve tensile strength, fracture toughness, thermal ability, barrier properties, and electrical properties [11–13]. Moreover, chemical treatments of CNTs, such as the –OH functionalization, make them the best option nanofillers for the fabrication of starch nanocomposite films [14]. However, many studies found that CNTs tend to agglomerate when used as reinforcement in starch biopolymers due to high surface area and low bonding between starch and the CNTs [12,13,15,16]

In this study, arrowroot starch was employed as the primary biopolymer for fabricating the nanocomposite films. The CNTs served as nanofillers to enhance arrowroot matrix, since hydrogen bonding between CNTs and the ARS matrix is expected to increase interfacial adhesion and mechanical performance of the composites. ARS/CNT nanocomposite films with CNTs content varying from 0 to 1.0 wt% were fabricated using solution casting method. The effects of CNTs' content on the properties of the nanocomposites were investigated by morphology, thickness, density, water content, moisture absorption, contact angle (CA), Fourier Transform Infrared (FTIR), X-ray Diffraction (XRD), thermal, and mechanical properties.

2 Materials and methods

2.1 Materials

The ARS was purchased from MH Food Matahari Sdn. Bhd. The multi-walled CNTs were purchased from Times Nano Chengdu Organic Chemicals Co. Ltd (purity > 90 wt%; outer diameter was in the range 10–30 nm; length was in the range 10–30 μm, specific surface area >140 m^2/g, and electrical conductivity >10^2 s/cm). Glycerol and sorbitol purchased from R&M chemicals provided by Evergreen Sdn. Bhd, Malaysia were employed in the study.

2.2 Preparation of CNTs/ARS nanocomposite films

Plasticized ARS/CNTs nanocomposite films were produced *via* the solution casting technique. The solution of CNTs (0–1.0 wt% on the starch basis) were prepared by mixing with 170 mL of distilled water and sonicating at 40 kHz and 180 W (Digital Pro+, Malaysia) for 30 min to disperse the CNTs in the solution and prevent the agglomeration. Then, 10 g of ARS and plasticizer (30% on the starch content) were mixed with the CNTs solution and stirred for 15 min at 85°C and 500 rpm using a magnetic stirrer (Huanghua Faithful Instrument Co. Ltd) for the starch to be gelatinized. This approach aimed to guarantee the consistent degradation of the starch granule and the concomitant formation of homogenous dispersion. The ratio of plasticizers (sorbitol and glycerol ratio) used was 1:1. The film-forming solution was thereafter allowed to cool and subjected to a vacuum to eliminate air bubbles prior to casting 50 g of the suspension onto each 13.5 cm diameter Petri dish. Then, the films were left to dry in the oven (Model-101-0A, Huanghua Faithful Instrument Co. Ltd) for 18 h at a set temperature of 45°C. The nanocomposite film with different loading concentrations of 0, 0.25, 0.5, and 1.0 wt% CNTs were denoted as ARS, ARS/CNTs-0.25, ARS/CNTs-0.5, and ARS/CNTs-1.0, respectively. Following 18 h of drying, ARS/CNT films were detached and preserved at 23 ± 2°C with a relative humidity (RH) of 50 ± 1% in a controlled environment for 7 days. Table 1 displays the composition of ARS/CNTs nanocomposite films.

Table 1: Composition of ARS/CNT films

No.	Starch (g)	CNTs (%)	Sorbitol and glycerol (1:1) (%)	Sample code
1	10	0	30	ARS
2	10	0.25	30	ARS/CNTs-0.25
3	10	0.5	30	ARS/CNTs-0.5
4	10	1	30	ARS/CNTs-1.0
Standard deviation		0.71		

2.3 Field emission scanning electron microscopy (FESEM)

The samples were coated with platinum *via* sputtering to enhance the electrical conductivity and improve surface morphology observation. The FESEM (JEOL JSM-7600F) observation was conducted at a voltage of 5 kV to examine the morphology of the films.

2.4 Film thickness

The film's thickness was assessed at six separate positions, and the average value was determined. Digital micrometer screw gauge (Mahr GmbH Esslingen, Model 40 EX German, precision 0.001 mm) was used to analyze the thickness.

2.5 Density

The density of the nanocomposite films was analyzed using densimeter (Mettler-Toledo (M) Sdn. Bhd). A film sample of 20 mm × 20 mm was used to ascertain the film density in accordance with ASTM D792-13 [17]. Ethanol was utilized as an alternative for distilled water as the immersion agent due to the inherently hydrophilic nature of the films. The specimen was preserved in a desiccator for 7 days to dehydrate. The dry mass of each film and the volume of fluid displaced upon submerging the films, denoted as m and V, respectively, were computed using equation (1). The procedure was repeated six times, and average value was computed.

$$\rho = \frac{m}{V}. \tag{1}$$

2.6 Water content

The water content was evaluated with ASTM D 644-94(1994). The original weight (w1) was recorded and then put in the oven for 24 h at 105°C. The sample was weighed again post-drying to ascertain the final weight (w2). The weight loss ratio during the drying process was calculated using equation (2). The average water content was calculated from five specimen sets.

$$\text{Water content}(\%) = \frac{\text{w1} - \text{w2}}{\text{w2}} \times 100. \tag{2}$$

2.7 Moisture absorption

The drying oven operated for 20 h to achieve a steady weight of the films. The desiccated samples were maintained in a room at 75% humidity and 25 °C for 6 h. The samples were measured using a precision balance every 30 min. The sample's moisture absorption was determined using equation (3).

$$\text{Moisture absorption}(\%) = \frac{\text{M}f - \text{M1}}{\text{M}f} \times 100. \tag{3}$$

2.8 CA

The CA of the film's surface was measured using a Theta Lite (Biolin Scientific, Sweden). The samples were measured by affixing them to the holder and employing the sessile drop technique to deposit water on the sample surface. The result was recorded for 10 s, followed by an immediate photograph.

2.9 FTIR analysis

A sheet film was scanned at a resolution of 4 cm^{-1}, covering the range from 4,000 to 500 cm^{-1} using the IR spectrometer (PerkinElmer, Spectrum, USA). The KBr-disk preparation method was used in this work. The Origin software was utilized to accurately determine the location of the characteristic peaks.

2.10 XRD

The XRD of the nanocomposite films were analyzed using a Rigaku SmartLab (Rigaku, Tokyo, Japan) equipped with CuKα radiation (λ = 0.1541 nm) throughout the 2θ range of 5°–40°. Subsequently, the assessment of the crystallinity index of the samples, I_{cr}, was facilitated by using the Segal method (1959), as shown in equation (4).

$$I_{cr} = \frac{I_{002} - I_{am}}{I_{002}} \times 100. \tag{4}$$

2.11 Thermal-gravimetric analysis (TGA)

The thermal analysis of the nanocomposite films was performed through TGA and DTG using thermal analysis system TGA/DSC 3^{+} (Mettler Toledo, USA). The samples were tested from 20 to 800°C at 10°C/min in nitrogen atmosphere.

2.12 Tensile properties

The samples were stored in desiccator with 23 ± 2°C and RH of 53 ± 1% for 72 h until constant weight. The universal testing machine Instron 3365 (High Wycombe, England),

equipped with a 30 kg load cell, was used to assess the tensile characteristics of the sample. The tensile properties were assessed using the standard procedure specified in ASTM D882. Samples of film measuring 10 mm × 70 mm were made for this test with 2 mm/min cross head speed. The mean value was derived from five distinct sets of specimens.

3 Result and discussion

3.1 Morphology of nanocomposite films

The distribution of CNTs in starch-based biopolymer is crucial for the overall performance of the nanocomposites. CNTs, recognized for their remarkable strength, electrical conductivity, and extensive surface area, have the ability to significantly enhance the properties of starch when uniformly incorporated within its matrix. [18]. The procedure started with the de-agglomeration of CNTs, accomplished using the integration of mechanical stirring and ultrasonication techniques. In Figure 1, the FESEM pictures clearly illustrate the well-dispersed of CNTs throughout the matrix. The luminous points and lines denote the ends of CNTs [14].

Achieving effective distribution of CNTs in starch biopolymers is challenging due to the inherent inclination of CNTs to agglomerate because of strong van der Waals forces [19]. When well-dispersed as shown in Figure 1d, CNTs form a uniform network throughout the starch matrix, improving the load redistribution between the starch and CNTs, thereby enhancing the tensile strength, elasticity, and water barrier properties of ARS/CNTs nanocomposite [12]. The multiwalled CNTs can be clearly seen through Figure 1d, as in other studies [20,21]. When ARS serves as the biopolymer matrix, there is an absence of CNTs agglomeration, in contrast to other studies, which indicate that CNTs tend to agglomerate within the matrix. This occurrence may be related to the distinctive properties of ARS, including its elevated amylose content and gel-forming capabilities, which facilitate a more uniform dispersion of CNTs. The strong interaction between the amylose chains and CNTs helps maintain a homogeneous distribution throughout the matrix, preventing the formation of agglomerates. Moreover, the FTIR result shows that

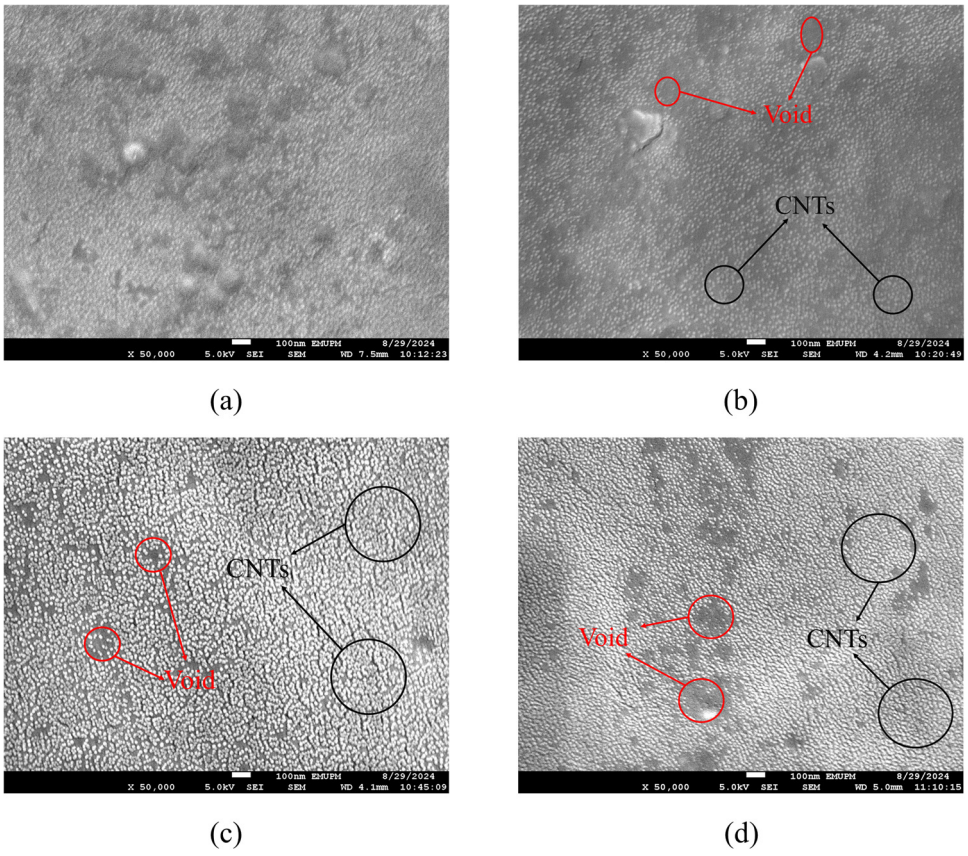

Figure 1: Morphology of ARS/CNTs nanocomposite films: (a) ARS, (b) ARS/CNTs-0.25, (c) ARS/CNTs-0.5, and (d) ARS/CNTs-1.0.

the arrowroot film has high OH– bond, which provides the space of the CNTs to interact with the arrowroot matrix. This result is also supported by mechanical properties, favorable water barrier, and thermal stability without the drawbacks of CNT clustering.

3.2 Density and thickness of the films

The density exhibited a positive correlation with the concentration of the nanofiller, displaying minimal fluctuations, as illustrated in Table 2. Films containing larger concentrations of CNTs demonstrated greater density values in comparison to films with lower concentrations. This finding could be ascribed to the chemical characteristics of the CNT, which possesses a significant number of hydroxyl groups on a substantial surface area of CNTs (>140 m^2/g). During processing, the strong connections between the CNTs were partially disturbed, resulting in the establishment of a strong new bond between the CNTs nanofiller and the ARS. The improved adhesion resulted in a decrease in the available space within the ARS biopolymer, causing it to become denser in comparison to pure starch. This study aligns with previous research by Slavutsky *et al.* [22], which showed that increasing the nanofiller content leads to a corresponding rise in the density of the nanocomposite film. The thickness of the films slightly increased on adding the CNTs loading in the film. This may be ascribed to the stringent regulation of the dry mass content per unit area of the film-forming solutions utilized during the casting process.

3.3 Moisture content

The water barrier characteristic is crucial in preventing the transfer of moisture between the film and its surroundings [23]. The moisture content of nanocomposite films made from ARS/CNTs with different concentrations of CNTs nanofiller ranged from 9.50 to 11.58%. Specifically, the moisture content for ARS and ARS/CNT films with CNT content of 0.25, 0.5, and 1.0% were 11.58, 9.97, 9.51, and 9.50% subsequently (Table 2). The amount of moisture in the film diminished as the content of CNTs in the film increased. This high moisture content of neat film can be ascribed to the hydrophilic nature of ARS, which contains polymers with multiple hydroxyl groups, with three hydroxyl groups per monomer [24]. Furthermore, there was a notable decrease in the moisture content of ARS biofilms at the concentrations of CNTs 0.5 and 1.0%. The reduction in hydrophilicity of the films was ascribed to the elevated concentration of CNTs loading due to the hydrophobic nature of the CNTs. This phenomenon can be attributed to the strong hydrogen bonding of the CNTs and the ARS matrix and bonding effectively hinders the interaction of water with the starch molecules [25].

3.4 Moisture absorption

Enhancing water resistance is crucial due to the significant water absorption propensity observed in starch systems, which is severely considered to be negative [26]. Figure 2 illustrates the moisture absorption of ARS and ARS/CNTs nanocomposite films. The figure indicates that the neat film made by ARS showed the highest moisture absorption because of its hydrophilic characteristics. Tarique *et al.* [27] reported that the ARS film is a hydrophilic biopolymer with significant swelling capacity. The reinforcement of CNTs resulted in a reduction in the water absorption capacity. After 30 min, the weight of the ARS film exhibited a noticeable rise of 3.36%. However, the ARS/CNT films did not show any noteworthy changes. Furthermore, the moisture absorption of ARS film with a 1.0% CNTs concentration was 7% lower than that of ARS film after 360 min. The moisture absorption phenomenon declined due to the intermolecular hydrogen bonding between the nanofiller and the ARS matrix. This leads to a decline in the quantity of available O–H groups, thereby diminishing the water molecules' diffusion capacity [1,28–30].

The higher concentration of the filler, improved dispersion of the nanofiller, and stronger bonding at the

Table 2: Physical properties of ARS and ARS/CNTs nanocomposite film with different concentrations of CNTs nanofiller

	Thickness (μm)	Density (g/cm^3)	Moisture content (%)
ARS	152.8	1.830	11.58
ARS/CNTs-0.25	154.3	1.852	9.97
ARS/CNTs-0.5	154.2	1.854	9.51
ARS/CNTs-1.0	155.6	1.857	9.50

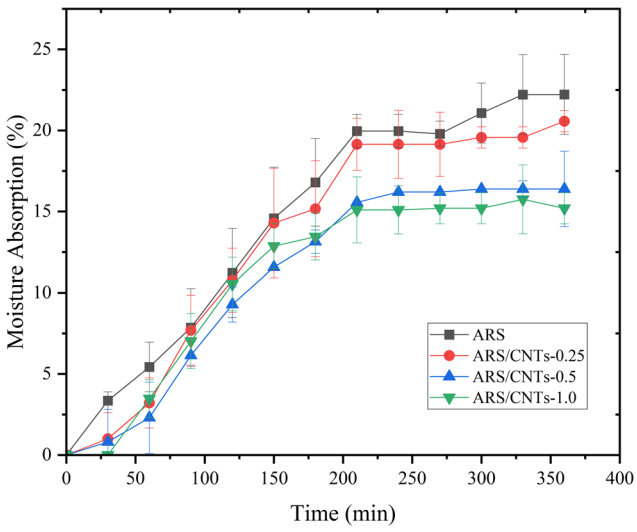

Figure 2: Moisture absorption of the ARS and ARS/CNTs nanocomposite films.

interface all contribute to barriers in diffusion, leading to longer and more convoluted pathways for water molecules. As a result, the permeability of water vapor decreases. The well-dispersed CNTs in the ARS reduces their free volume thereby causing improvements in the film resistance to the moisture [31].

3.5 CA

The surface hydrophobicity of a polymeric film signifies whether the surface is hydrophilic (<90°) or hydrophobic (>90°) [15,32]. Figure 3 shows the CA test from different CNTs content. As can be seen, the CA increases as the CNTs loading increases, with ARS (52.42°) becoming the lowest CA . When a water droplet comes into the surface, starch rapidly absorbs the water due to the water-soluble nature of the starch. The high CA resulted from the hydrophobic nature and the dispersion of the CNTs on the surface of the films, which prevent water from diffusing into the film surface. The CA image clearly showed that the surface hydrophobicity of the films greatly enhanced after incorporation of CNTs. Among the starch that had reinforced CNTs, the film containing 1% CNTs showed the highest CA with a value 93.81°, which improved by a value of 41.39° higher than neat film. This result is consistent with the study by Shahbazi *et al.* [25] while the CNTs loading increased, the CA of the film increased at the same time. This CA test also reduces the moisture absorption, as the same pattern was observed in this study. Similarly, the moisture content data (Table 3) confirms that increasing the CNTs loading enhances the hydrophobicity of the films.

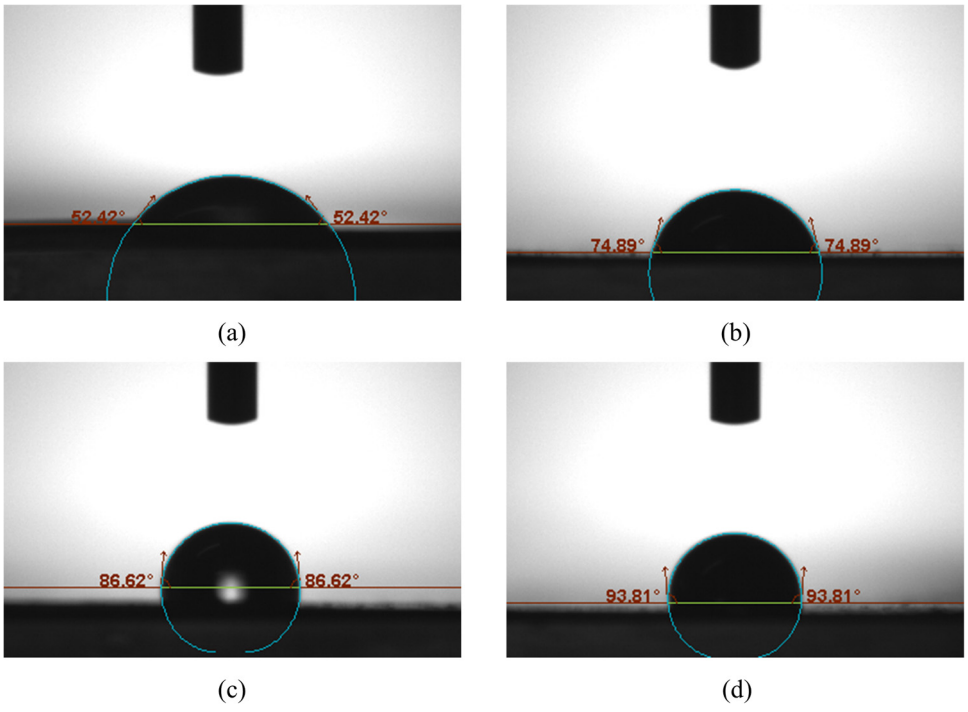

Figure 3: CA test of the film: (a) ARS, (b) ARS/CNTs-0.25, (c) ARS/CNTs-0.5, and (d) ARS/CNTs-1.0.

Table 3: TGA of the films

Sample	I stage: water evaporation			II stage: thermal degradation			Residual: char yield
	T_{onset} (°C)	T_{max} (°C)	Mass loss (%)	T_{donset} (°C)	T_d (°C)	Mass loss (%)	Mass loss (%)
ARS	21	121	6.0	283	312	78.4	1.9
ARS/CNTs-0.25	21	117	7.6	283	311	79.7	5.7
ARS/CNTs-0.5	23	126	7.1	283	311	80.5	8.2
ARS/CNTs-1.0	23	111	7.6	283	313	79.7	5.3

3.6 FTIR spectroscopy analysis

The functional groups of the films were analyzed using FTIR spectroscopy. It offers valuable insights into the presence of functional groups and aids in identifying molecular kinds and structures [33]. Figure 4 exhibits the FTIR of the nanocomposite films, showcasing different concentrations of CNTs. The ARS film, when seen at a wavenumber of 3,291 cm^{-1}, exhibited a broad peak that may be ascribed to the hydroxyl group (–OH) group. This observation is confirmed by the findings of Tarique *et al.* [34]. The peak at 2,924 cm^{-1} can be ascribed to the stretching of the C–H bond, whereas the smaller peak observed at 1,648 cm^{-1} may be attributed to the stretching of the C═O (carbonyl) bond. The peak at 1,361 cm^{-1} was the characteristic absorbance spectrum of O–C–H, C–C–H, and C–O–H groups on the starch chains [35]. Another wave at 1,006 cm^{-1} could be associated with the carbonyl (–C–O) existing functionality in C–O–C groups.

The FTIR of pure ARS films were indistinguishable from that of the nanocomposite films including ARS and CNTs. The inclusion of a tiny concentration of CNTs had a minimal impact on the chemical composition of the nanocomposite films, since no other peaks were seen. The –OH stretching peak of the neat ARS film shifted slightly to a higher wavenumber (3,293 cm^{-1}) with the addition of 0.25 wt% CNTs, suggesting a minor interaction between CNTs and the ARS matrix, possibly due to weak hydrogen bonding. However, at higher CNT concentrations, the –OH peak position remained unchanged (3,291 cm^{-1}), indicating no further effect on the molecular structure or hydrogen bonding [12].

3.7 XRD analysis

The XRD analysis of the nanocomposites was conducted to assess how varying CNT concentrations influenced the crystallinity of the nanocomposite films shown in Figure 5. All films exhibit a diffraction pattern featuring a prominent peak at 2θ = 24.2°. After the introduction of CNTs (0–1%), the crystalline pattern remained unchanged, and the diffraction peaks continued to exist at the same positions, attributing

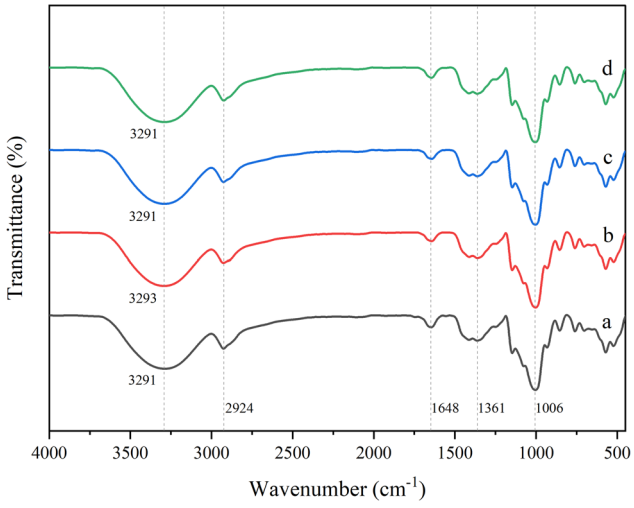

Figure 4: FTIR spectra of (a) ARS, (b) ARS/CNTs-0.25, (c) ARS/CNTs-0.5, and (d) ARS/CNTs-1.0.

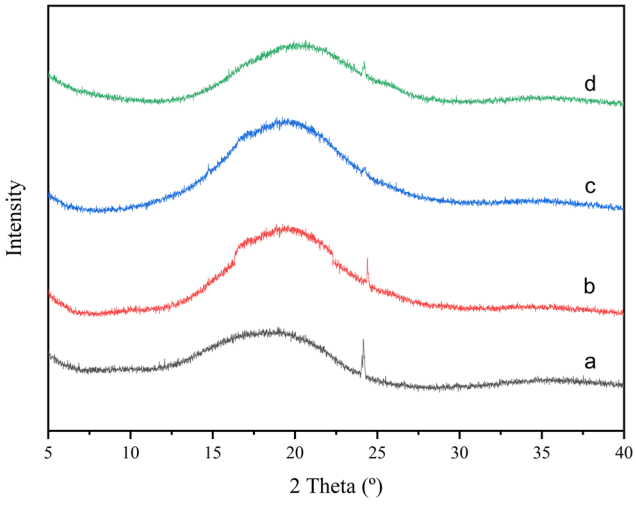

Figure 5: XRD pattern of (a) ARS, (b) ARS/CNTs-0.25, (c) ARS/CNTs-0.5, and (d) ARS/CNTs-1.0.

to the low content of the CNTs, this finding is similar to that in the research by Liu *et al.* [12].

The neat arrowroot film exhibited the highest crystallinity index (I_{cr}) (22%), which decreased after the incoporation of CNTs (0.25–1.0%). The crystallinity of the film with 0.5% CNTs was 3%, while with 1% of CNT content, there is a slight increase in I_{cr} (9%). This remarkable phenomenon may be ascribed to the ability of CNTs to disrupt the crystalline construction of ARS, along with their effective dispersion emerging from the extensive surface area of CNTs. The reduction in peak intensity is attributed to the decrease in the crystallinity of the sample [36].

3.8 Thermal analysis

TGA was utilized to examine the effect of nanofillers and the thermal resistance characteristics of CNTs within the arrowroot matrix. The thermal degradation of the films was evaluated through TGA and DTG across temperatures 20–800°C, as depicted in Figure 6. Table 3 illustrates that there is no significant mass loss in the CNT-loaded samples compared to neat starch. This suggests that the incorporation of CNTs at low concentrations (≤1.0 wt%) does not substantially affect the bulk thermal degradation behavior of the films. While CNTs may interact with the ARS matrix, the interfacial adhesion appears insufficient to alter the overall decomposition profile in a measurable way. As such, the observed thermal response remains primarily ruled by the ARS matrix, with CNTs contributing more noticeably to residual char formation rather than shifting degradation stages [25,37–39]. The initial degradation of about 6.0% for pure ARS begins at 120°C, attributed to the water molecules evaporation, and a comparable degradation pattern is noted in ARS/CNTs nanocomposite films. The significant mass loss of 78.4% observed between 312 and 349°C can be ascribed to the pyrolysis of the polymer chain and the degradation of saccharide rings, a process triggered by the thermal decomposition of the arrowroot polymer [40,41]. This situation occurred in all other film samples.

The thermal decomposition curve indicates that T_{max} of ARS/CNTs-0.25 (311°C) increased on adding CNTs loading of 1% and reached temperature 312°C. The addition of CNTs to the ARS matrix enhanced the thermal stability of the nanocomposite films. The improvement in the thermal stability of the nanocomposite through the introduction of CNTs is consistent with previous studies [12,14,42]. Char yield is the remaining substance after the pyrolysis process. The char

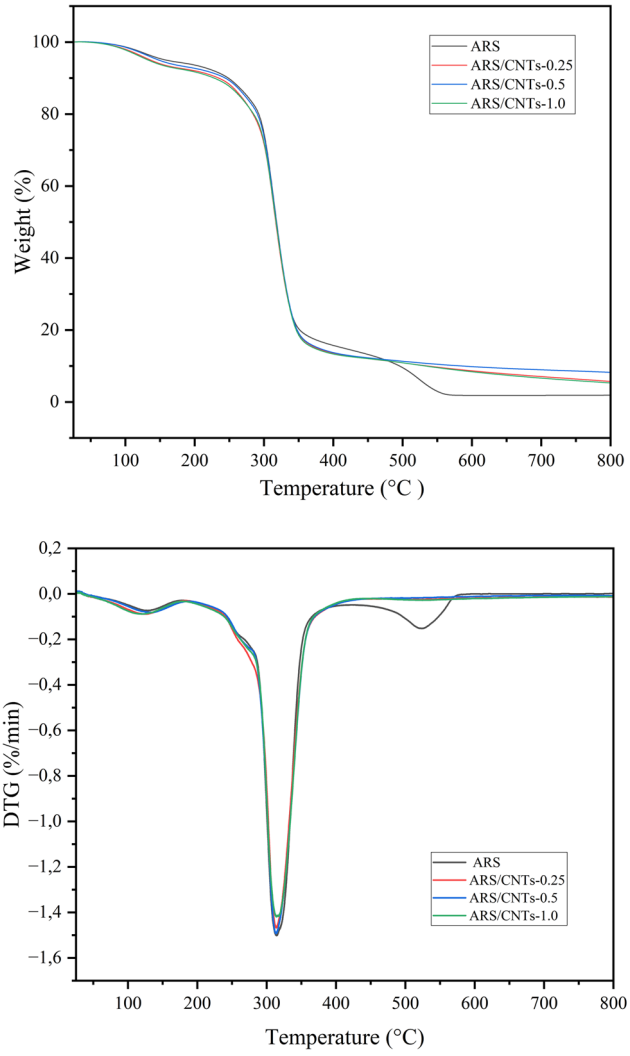

Figure 6: TGA and DTG of the ARS/CNTs nanocomposite films at different concentrations.

content of nanocomposites was found to augment with the incorporation of CNTs, where the incorporation of 0.5% CNTs into ARS resulted in the most significant increase, reaching 8.2% from 1.9% (neat ARS). The mass loss increased due to initial degradation effects. Table 3 shows that the first stage of mass loss was less than that of ARS/CNTs-0.25 and ARS/CNTs-1.0. The CNT cluster inside the matrix may be the cause of this phenomenon. Nevertheless, at 1% CNT, the greater network formation and dispersion improved thermal stability, limiting volatile breakdown products and lowering mass loss by serving as a heat barrier. The improved thermal stability of the films compared to the ARS may be associated with the substantial carbonate content in the CNTs, which correlates well with the results of thermal degradation of the nanocomposites.

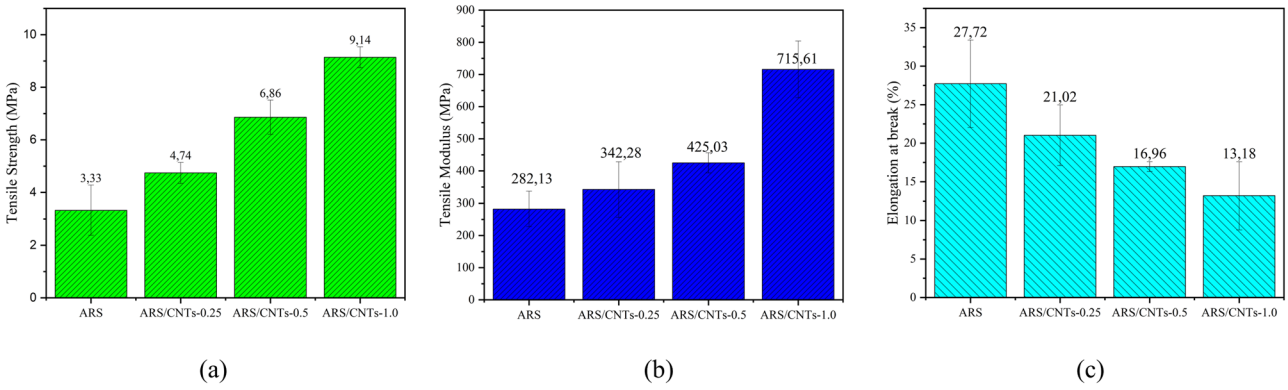

Figure 7: Effect of CNTs concentration on the (a) tensile strength, (b) tensile modulus, and (c) elongation at break nanocomposite films.

3.9 Tensile properties

The combination of CNTs and the ARS resulted in a notable enhancement of the tensile strength and modulus elasticity of the films, owing to the efficient stress transfer between the two materials [43]. Nanofiller with a high surface area, such as CNTs (specific surface Area > 140 m^2/g) contribute to improved mechanical properties. The nanofillers facilitate the establishment of adhesion within the nanocomposite during the dehydration step of the manufacturing process. Increasing the concentration of nanofillers may enhance the mechanical properties of the films [1].

According to Figure 7, the nanocomposite films demonstrated a consistent improvement in tensile strength and Young's modulus with the increasing concentration of CNTs in the matrix films. The tensile strength of the film rose after the addition of CNTs and reached 9.14 ± 0.39 MPa when the CNTs concentration was 1.0%. This value is approximately 174% greater than the tensile strength of the film without CNTs, which was 3.33 ± 0.95 MPa. The increase in tensile strength was attributed the efficient and even distribution of CNTs and their strong interfacial bonding enhanced stress transfer efficiency and load-bearing capacity from the ARS matrix to the fillers [44]. Compared with the findings of Liu *et al.* [43], where the addition of 1.0% CNTs resulted in a tensile strength about 7 MPa, the present study provides a higher mechanical performance. Moreover, the ultrasonic process generates enough energy that breaks the clusters of CNTs and assists in their uniform dispersion in the nanocomposite films [45]. The Young's modulus of the film increased dramatically when CNTs were present. It went from 282.13 ± 54.86 MPa for the film without CNTs to 715.61 ± 88.15 MPa for the film with 1.0% CNTs concentration. The reinforcing effect must correspond with the interaction between the fillers and the matrix. The CNT filler is anticipated to establish more strong interactions with the ARS matrix due to the CNTs' ability to build superior hydrogen bond interactions with starch [13].

However, regarding the film's elongation at break, following a minor increase at a CNT content of 0.25%, the value subsequently diminished with additional increments in CNT content. With the increase in CNTs content up to 1%, the elongation at break of the sample reduced from 27.7% of neat ARS film to 13.2% of ARS/CNTs-1.0 nanocomposite, it is because the spatial restraint of starch chains movement yielded increasingly brittle samples [13]. Furthermore, the insertion of CNTs caused the disruption of the orderly hydrogen bonding in the ARS, resulting in a decrease in the entanglement of the ARS chains. Additionally, the presence of the crystalline domain and the micro-ordered zones on a larger scale limited the movement of ARS chains and reduced the available space within the films.

4 Conclusion

This study presents the successful production of ARS-based films reinforced with multi-walled CNTs and developed through ultrasonication and the solution casting method. The addition of CNTs into the ARS matrix with good dispersion successfully enhanced the water barrier properties and the hydrophobicity of the nanocomposite films. The increase in CNTs content led to the disruption of hydrogen bonding in ARS and caused a decline in the short-range molecular conformation of ARS. Furthermore, the incorporation of CNTs significantly improved both the tensile strength and modulus. The maximum values were observed with the highest filler loading in the ARS/CNTs-1.0 nanocomposite film. The use of ARS facilitates effective dispersion of CNTs within the matrix. Consequently, the ARS improved the biocompatibility of the multi-walled CNTs, whereas the CNTs demonstrated remarkable

mechanical, thermal, and water barrier properties. The potential applications of nanocomposites encompass biosensors, medical devices, agriculture, drug delivery systems, and serving as a filler in biopolymer matrix composites.

Acknowledgments: The authors would like to express their sincere appreciation to the Ministry of Higher Education Malaysia for the financial support provided through the Fundamental Research Grant Scheme (FRGS/1/2023/TK09/UPM/01/3) at Universiti Putra Malaysia.

Funding information: This study received funding from the Ministry of Higher Education Malaysia (MoHE) under the Fundamental Research Grant FRGS/1/2023/TK09/UPM/01/3.

Author contributions: All authors have accepted responsibility for the entire content of this manuscript and approved its submission.

Conflict of interest: The authors state no conflict of interest.

Data availability statement: The datasets generated and/or analyzed during the current study are available from the corresponding author on reasonable request.

References

[1] Ilyas RA, Sapuan SM, Ishak MR, Zainudin ES. Development and characterization of sugar palm nanocrystalline cellulose reinforced sugar palm starch bionanocomposites. Carbohydr Polym. 2018;202:186–202. doi: 10.1016/j.carbpol.2018.09.002.

[2] Othman SH, Shapi'i RA, Ronzi NDA. Starch biopolymer films containing chitosan nanoparticles: A review. Carbohydr Polym. 2024;329:121735. doi: 10.1016/j.carbpol.2023.121735.

[3] Jailani A, Hidzer MH, Firdaus AHM, Sapuan SM, Zainudin ES, Atiqah A, et al. Enhancing polyvinyl alcohol (PVA) nanocomposites: Key properties, applications and challenges in advanced engineering. Def Technol. 2025. doi: 10.1016/j.dt.2025.05.020.

[4] Yu X, Chen L, Jin Z, Jiao A. Research progress of starch-based biodegradable materials: A review. J Mater Sci. 2021;56:11187–208. doi: 10.1007/s10853-021-06063-1.

[5] Averous L, Boquillon N. Biocomposites based on plasticized starch: Thermal and mechanical behaviours. Carbohydr Polym. 2004;56:111–22. doi: 10.1016/j.carbpol.2003.11.015.

[6] Sandoval Gordillo CA, Ayala Valencia G, Vargas Zapata RA, Agudelo Henao AC. Physicochemical characterization of arrowroot starch (Maranta arundinacea Linn) and glycerol/arrowroot starch membranes. Int J Food Eng. 2014;10:727–35. doi: 10.1515/ijfe-2014-0122.

[7] Tarique J, Sapuan SM, Khalina A, Ilyas RA, Zainudin ES. Thermal, flammability, and antimicrobial properties of arrowroot (Maranta arundinacea) fiber reinforced arrowroot starch biopolymer composites for food packaging applications. Int J Biol Macromol. 2022;213:1–10. doi: 10.1016/j.ijbiomac.2022.05.104.

[8] Sanyang ML, Sapuan SM, Jawaid M, Ishak MR, Sahari J. Effect of sugar palm-derived cellulose reinforcement on the mechanical and water barrier properties of sugar palm starch biocomposite films. BioResources. 2016;11:4134–45. doi: 10.15376/biores.11.2.4134-4145.

[9] Paul A, Sharma SS Biopolymer-based nanocomposites. In: Thomas S AR A, Jose Chirayil C, Thomas B, editors. Handbook of biopolymers. Singapore: Springer Nature Singapore; 2023. p. 523–50. doi: 10.1007/978-981-19-0710-4_19.

[10] Dubey R, Dutta D, Sarkar A, Chattopadhyay P. Functionalized carbon nanotubes: Synthesis, properties and applications in water purification, drug delivery, and material and biomedical sciences. Nanoscale Adv. 2021;3:5722–44. doi: 10.1039/d1na00293g.

[11] Mohammadsalih ZG, Sadeq NS. Structure and properties of polystyrene/graphene oxide nanocomposites. Fuller Nanotubes Carbon Nanostruct. 2022;30:373–84. doi: 10.1080/1536383X.2021.1943367.

[12] Liu S, Li X, Chen L, Li L, Li B, Zhu J. Understanding physicochemical properties changes from multi-scale structures of starch/CNT nanocomposite films. Int J Biol Macromol. 2017;104:1330–7. doi: 10.1016/j.ijbiomac.2017.05.174.

[13] Cheng J, Zheng P, Zhao F, Ma X. The composites based on plasticized starch and carbon nanotubes. Int J Biol Macromol. 2013;59:13–9. doi: 10.1016/j.ijbiomac.2013.04.010.

[14] Swain SK, Pradhan AK, Sahu HS. Synthesis of gas barrier starch by dispersion of functionalized multiwalled carbon nanotubes. Carbohydr Polym. 2013;94:663–8. doi: 10.1016/j.carbpol.2013.01.056.

[15] Alves Z, Abreu B, Ferreira NM, Marques EF, Nunes C, Ferreira P. Enhancing the dispersibility of multiwalled carbon nanotubes within starch-based films by the use of ionic surfactants. Carbohydr Polym. 2021;273:118531. doi: 10.1016/j.carbpol.2021.118531.

[16] Yan L, Chang PR, Zheng P. Preparation and characterization of starch-grafted multiwall carbon nanotube composites. Carbohydr Polym. 2011;84:1378–83. doi: 10.1016/j.carbpol.2011.01.042.

[17] Standard A. D792-13, 2013. Standard test methods for density and specific gravity (relative density) of plastics by displacement. West Conshohocken: ASTM International; 2013. doi: 10.1520/D0792-13 n.d.

[18] Nurazzi NM, Sabaruddin FA, Harussani MM, Kamarudin SH, Rayung M, Asyraf M, et al. Mechanical performance and applications of CNTs reinforced polymer composites—A review. Nanomaterials (Basel, Switz). 2021;11:2186. doi: 10.3390/nano11092186.

[19] Siddiqui VU, Sapuan SM, Hassan MR. Innovative dispersion techniques of graphene nanoplatelets (GNPs) through mechanical stirring and ultrasonication: Impact on morphological, mechanical, and thermal properties of epoxy nanocomposites. Def Technol. 2025;43:13–25. doi: 10.1016/j.dt.2024.04.018.

[20] Mallakpour S, khodadadzadeh L. Ultrasonic-assisted fabrication of starch/MWCNT-glucose nanocomposites for drug delivery. Ultrason Sonochem. 2018;40:402–9. doi: 10.1016/j.ultsonch.2017.07.033.

[21] Yurdakul H, Durukan O, Seyhan AT, Celebi H, Oksuzoglu M, Turan S. Microstructural characterization of corn starch-based porous thermoplastic composites filled with multiwalled carbon

nanotubes. J Appl Polym Sci. 2013;127:812–20. doi: 10.1002/app.37794.
[22] Slavutsky AM, Bertuzzi MA, Armada M. Water barrier properties of starch-clay nanocomposite films. Braz J Food Technol. 2012;15:208–18. doi: 10.1590/s1981-67232012005000014.
[23] Syafiq R, Sapuan SM, Zuhri MRM. Antimicrobial activity, physical, mechanical and barrier properties of sugar palm based nanocellulose/starch biocomposite films incorporated with cinnamon essential oil. J Mater Res Technol. 2021;11:144–57. doi: 10.1016/j.jmrt.2020.12.091.
[24] Wurm F, Rietzler B, Pham T, Bechtold T. Multivalent ions as reactive crosslinkers for biopolymers—A review. Molecules. 2020;25:1840. doi: 10.3390/molecules25081840.
[25] Shahbazi M, Rajabzadeh G, Sotoodeh S. Functional characteristics, wettability properties and cytotoxic effect of starch film incorporated with multi-walled and hydroxylated multi-walled carbon nanotubes. Int J Biol Macromol. 2017;104:597–605. doi: 10.1016/j.ijbiomac.2017.06.031.
[26] Gao W, Dong H, Hou H, Zhang H. Effects of clays with various hydrophilicities on properties of starch–clay nanocomposites by film blowing. Carbohydr Polym. 2012;88:321–8. doi: 10.1016/j.carbpol.2011.12.011.
[27] Tarique J, Sapuan SM, Zainudin ES, Khalina A, Ilyas RA. Degradation behaviour of arrowroot fibre (Maranta arundinacea) reinforced arrowroot starch biocomposite films. J Res Nanosci Nanotechnol. 2022;5:98–102. doi: 10.37934/jrnn.5.1.98102.
[28] Abral H, Hartono A, Hafizulhaq F, Handayani D, Sugiarti E, Pradipta O. Characterization of PVA/cassava starch biocomposites fabricated with and without sonication using bacterial cellulose fiber loadings. Carbohydr Polym. 2019;206:593–601. doi: 10.1016/j.carbpol.2018.11.054.
[29] Hafizulhaq F, Abral H, Kasim A, Arief S, Affi J. Moisture absorption and opacity of starch-based biocomposites reinforced with cellulose fiber from bengkoang. Fibers. 2018;6:62. doi: 10.3390/fib6030062.
[30] Abral H, Ariksa J, Mahardika M, Handayani D, Aminah I, Sandrawati N, et al. Highly transparent and antimicrobial PVA based bionanocomposites reinforced by ginger nanofiber. Polym Test. 2020;81:106186. doi: 10.1016/j.polymertesting.2019.106186.
[31] Glaskova-Kuzmina T, Aniskevich A, Martone A, Giordano M, Zarrelli M. Effect of moisture on elastic and viscoelastic properties of epoxy and epoxy-based carbon fibre reinforced plastic filled with multiwall carbon nanotubes. Compos Part A: Appl Sci Manuf. 2016;90:522–7. doi: 10.1016/j.compositesa.2016.08.026.
[32] Shahbazi M, Rajabzadeh G, Ettelaie R, Rafe A. Kinetic study of κ-carrageenan degradation and its impact on mechanical and structural properties of chitosan/κ-carrageenan film. Carbohydr Polym. 2016;142:167–76. doi: 10.1016/j.carbpol.2016.01.037.
[33] Lou Y, Hao X, Liao L, Zhang K, Chen S, Li Z, et al. Recent advances of biomass carbon dots on syntheses, characterization, luminescence mechanism, and sensing applications. Nano Sel. 2021;2:1117–45. doi: 10.1002/nano.202000232.
[34] Tarique J, Sapuan SM, Khalina A. Effect of glycerol plasticizer loading on the physical, mechanical, thermal, and barrier properties of arrowroot (Maranta arundinacea) starch biopolymers. Sci Rep. 2021;11:1–17. doi: 10.1038/s41598-021-93094-y.
[35] Iizuka K, Aishima T. Starch gelation process observed by FT-IR/ATR spectrometry with multivariate data analysis. J Food Sci. 1999;64:653–8. doi: 10.1111/j.1365-2621.1999.tb15104.x.
[36] Jose J, De SK, AlMa'adeed MA-A, Dakua JB, Sreekumar PA, Sougrat R, et al. Compatibilizing role of carbon nanotubes in poly (vinyl alcohol)/starch blend. Starch - Stärke. 2015;67:147–53. doi: 10.1002/star.201400074.
[37] Ortega-Toro R, Santagata G, Gomez d'Ayala G, Cerruti P, Talens Oliag P, Chiralt Boix MA, et al. Enhancement of interfacial adhesion between starch and grafted poly(ε-caprolactone). Carbohydr Polym. 2016;147:16–27. doi: 10.1016/j.carbpol.2016.03.070.
[38] Perumal N, Sreekantan S, Hamid ZAA, Rusli A, Bhubalan K, Appaturi JN. Effect of plasticizer and compatibilizer on properties of polybutylene adipate-co-terephthalate (PBAT) with acetylated starch. J Polym Environ. 2024;32:289–302. doi: 10.1007/s10924-023-02964-1.
[39] Tian Y, Li Y, Xu X, Jin Z. Starch retrogradation studied by thermogravimetric analysis (TGA). Carbohydr Polym. 2011;84:1165–8. doi: 10.1016/j.carbpol.2011.01.006.
[40] Sanyang ML, Sapuan SM, Jawaid M, Ishak MR, Sahari J. Development and characterization of sugar palm starch and poly (lactic acid) bilayer films. Carbohydr Polym. 2016;146:36–45. doi: 10.1016/j.carbpol.2016.03.051.
[41] Abral H, Basri A, Muhammad F, Fernando Y, Hafizulhaq F, Mahardika M, et al. A simple method for improving the properties of the sago starch films prepared by using ultrasonication treatment. Food Hydrocoll. 2019;93:276–83. doi: 10.1016/j.foodhyd.2019.02.012.
[42] Ciambelli P, Sarno M, Gorrasi G, Sannino D, Tortora M, Vittoria V. Preparation and physical properties of carbon nanotubes–PVA nanocomposites. J Macromol Sci Part B. 2005;44:779–95. doi: 10.1080/00222340500251410.
[43] Liu Z, Zhao L, Chen M, Yu J. Effect of carboxylate multi-walled carbon nanotubes on the performance of thermoplastic starch nanocomposites. Carbohydr Polym. 2011;83:447–51. doi: 10.1016/j.carbpol.2010.08.007.
[44] Ning N, Fu S, Zhang W, Chen F, Wang K, Deng H, et al. Realizing the enhancement of interfacial interaction in semicrystalline polymer/filler composites via interfacial crystallization. Prog Polym Sci. 2012;37:1425–55. doi: 10.1016/j.progpolymsci.2011.12.005.
[45] Kundalwal SI, Rathi A. Improved mechanical and viscoelastic properties of CNT-composites fabricated using an innovative ultrasonic dual mixing technique. J Mech Behav Mater. 2020;29:77–85. doi: 10.1515/jmbm-2020-0008.